Importance of the Goodman jack to evaluate the Permeability of the Rock Mass by applying Flow Net

Importance du Goodman jack pour évaluer la perméabilité du massif rocheux en appliquant le réseau d'écoulement

Julio Chable[1#], *Adrian Ferriño*[2], and *Jorge Lopez*[3]

[1]JC Estudios Geotécnicos, Tlajomulco de Zuñiga, Jalisco, México
[2]Universidad Autónoma de Nuevo León, Monterrey, Nuevo Leon, México
[3]Comision Federal de Electricidad, Ciudad de México, México
[#] julio.chable001@gmail.com

ABSTRACT

The Goodman Jack test is a fundamental tool for evaluating the deformability of rock masses, allowing engineers to define the appropriate treatments during the construction process. One of the key factors to consider in large-scale infrastructure projects, such as the foundation of water storage dams, is the permeability of the terrain. Water infiltration can compromise structural stability, making it essential to anticipate and quantify permeability values before and during construction. To achieve an accurate evaluation, the following in situ correlations are performed: geomechanical classifications of the rock mass, Lugeon-type permeability tests, and flow network modeling to estimate water infiltration This analysis allows for the selection of optimal treatment strategies for the rock mass, ensuring cost and time reduction in project execution, higher efficiency in waterproofing works, and improved quality and stability of the structure.

RESUME

Le test de Gato Goodman est un outil fondamental pour l'évaluation de la déformabilité du massif rocheux, permettant de définir les traitements appropriés au cours du processus de construction. L'un des facteurs clés à prendre en compte dans les projets d'infrastructure de grande envergure, comme les fondations de barrages de stockage d'eau, est la perméabilité du sol. L'infiltration d'eau peut compromettre la stabilité structurelle, il est donc essentiel d'anticiper et de quantifier les valeurs de perméabilité avant et pendant la construction. Pour réaliser une évaluation précise, les corrélations in situ suivantes sont effectuées: classifications géomécaniques du massif rocheux, tests de perméabilité de type Lugeon et modélisation du réseau d'écoulement pour estimer l'infiltration de l'eau.
Cette analyse permet de sélectionner des stratégies de traitement optimales pour le massif rocheux, garantissant une réduction des coûts et des délais d'exécution, une meilleure efficacité des travaux d'étanchéité et une optimisation de la qualité et de la stabilité de la structure.

Keywords: characterization, discontinuities, intact, mass, rock, permeability.

1. Objetive

This article highlights the importance of conducting in situ tests in rock formations, including the Goodman Jack test to assess the deformability of the rock mass, Lugeon permeability tests to determine water infiltration in the foundation, and geomechanical surveys to characterize the structural quality of the rock mass. These studies are complemented by laboratory tests conducted throughout the dam foundation to correlate results and obtain an accurate terrain diagnosis. Based on the collected data, a flow network analysis is performed, allowing the correlation of mechanical and permeability tests with the maximum filtration rate beneath the dam structure. This is crucial for selecting the most suitable treatments for the rock mass, optimizing stability, safety, and efficiency during construction. (Figure 1).
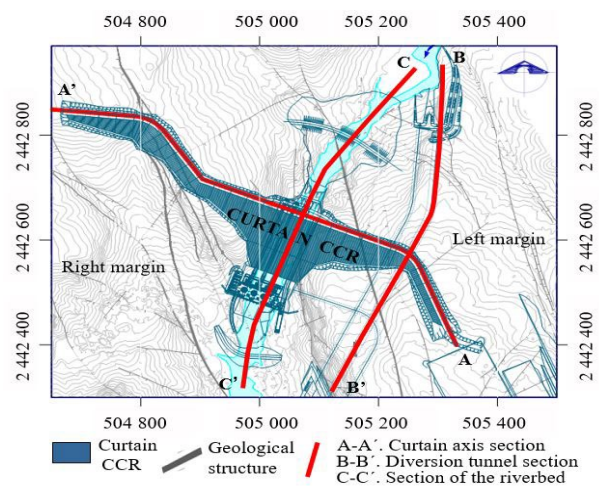

Figure 1. Location of the containment work of the Dam.

2. Objetive

To synthesize the geomechanical characterization methodology of the rock mass, a process diagram was created, specifying the activities to be developed in each work area (Figure 2).
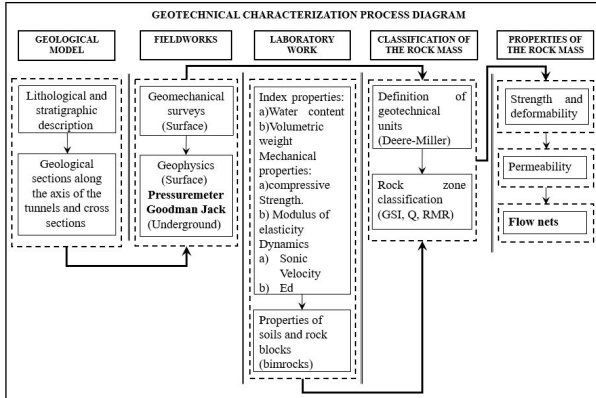

Figure 2. Geotechnical characterization process diagram.

3. Geological model

3.1. Lithology

The study site is geologically located in the Ignimbrite sequence of the Nayar, composed of the Corapan and Las Cruces formations, formed by rocks of volcanic origin with an intercalation of tuffs and ignimbrites. Regarding lithology, the Corapan unit is formed by Ignimbrites, Tm-ci1 (Ug-1b) of light gray color, pyroclastic texture, composed of potassium feldspars, plagioclases, quartz and ferromagnesian, followed by the Reddish Tuff,Tm-ct1 (Ug-1c) of reddish color, pyroclastic texture, compact structure with angular fragments of rhyolitic ignimbrite of various sizes, until reaching the Las Cruces unit, in its upper part, Tm-ic2 (Ug-2a) is made up of light gray rhyolitic lithic ignimbrites of fine-grained pyroclastic texture and is underlain by the vesicular Ignimbrite with cavities and vesicles mostly filled, see Figures 3, 4 and 5.
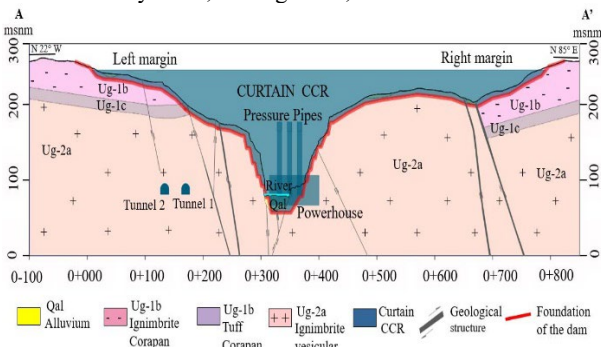

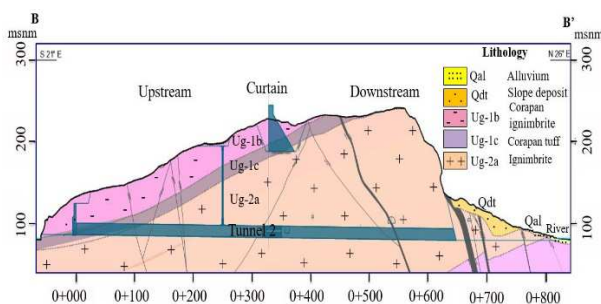**Figure 3.** Geological section along the axis of the dam.

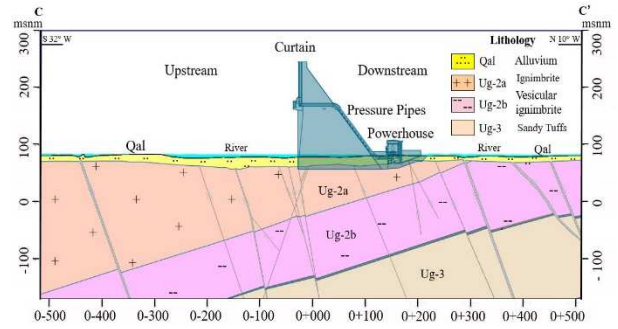**Figure 4.** Geological section along the axis of the diversion tunnel.

Figure 5. Geological section along the axis of the riverbed.

3.2. Structural Geology

With the data obtained from the geological surveys in the area, the stereonet shown in figure 4 was elaborated. The fault and fracture systems at the site coincide with the orientations of the dominant systems at the regional level.
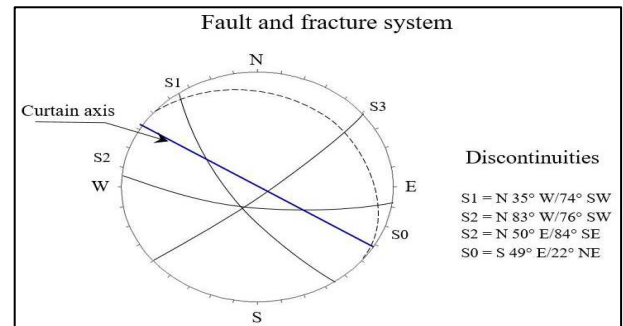

Figure 6. Geotechnical characterization process diagram.

4. Field work

During the fieldwork for geotechnical characterization, geomechanical surveys were carried out in the study area, identifying a rock zone. In the study zone, geomechanical surveys were carried out using the methodologies proposed by Bieniawski RMR, Barton Q. Barton N. (2002), Hoek, E. et al. (2002) and Morelli (2017). Similary, tests were carried out with the Schmidt hammer (sclerometer), on the surface of the healthy rock (R) and on the joints (r), by the correlations Miller 1965, Chable J. et al. 2022, for the different rock-rock contacts. Additionally, small-scale roughness (Figure 5), and large scale roughness, Figure 12 were evaluated.
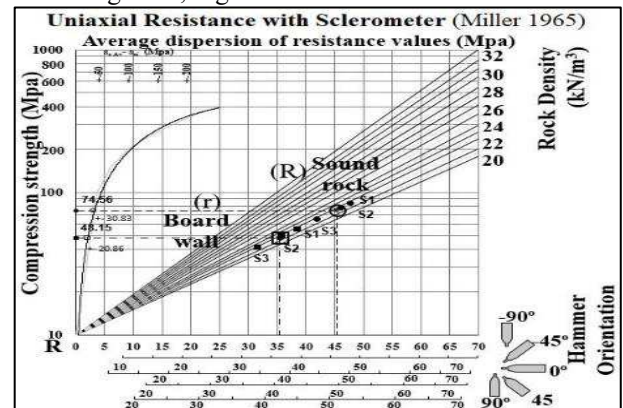

Figure 7. Abacus for calculating the JCS with the sclerometer in the field, from Miller 1965.

5. Laboratory work

In the laboratory work, healthy samples without alteration or fractures were selected to carry out compressive strength tests. this allowed to obtain the moduli of elasticity, as well as its dynamic properties with the primary and secondary velocity Vp and Vs, (Montiel E., Chable J., 2012).

5.1. Index properties

Table 1 presents the average values corresponding to the water content and the volumetric weight from laboratory results.

Table 1. Average values of index properties of intact rock

Lithology	Description	Volumetric weight kN/m3		Water content %
		γ ambient	γ saturated	
Ug-1b	Corapan Ignimbrite	21.20	21.93	5.33
Ug-1c	Corapan Rhyolitic Tuff	22.06	23.41	4.21
Ug-2a	Ignimbrite	21.50	22.78	5.77

5.2. Mechanical properties

To evaluate the stress-strain behavior of the intact rock, compressive strength (σ_{ci}) tests were performed to obtain the indirect (σ_t), as well as triaxial stress tests (σ_1, σ_3) moduli of elasticity (Et50), The average results by rock type are shown in Table 2.

Table 2. Average values of mechanical properties of intact rock

Lithology	Description	σ_t MPa	σ_c MPa	E_{t50} MPa	σ_1 MPa	σ_3 MPa
Ug-1b	Corapan Ignimbrite	5.97	67.2	19031	90.3	13.9
Ug-1c	Corapan Rhyolitic Tuff	6.60	66.6	18931	86.6	14.1
Ug-2a	Ignimbrite	6.14	76.1	21270	94.3	9.9

5.3. Dynamic properties

Similarly, in order to assess the degree of alteration of the rock, tests were carried out on the speed of propagation of elastic compression waves (Vp) and transverse (Vp), to determine the moduli dynamic (Ed) and Poisson parameter (μ), Table 3.

Table 3. Average values of dynamic properties of the intact rock

Lithology	Description	Velocity		E dynamic MPa	Relation of Poisson μ
		V_p m/s	V_s m/s		
Ug-1b	Corapan Ignimbrite	3140	2888	15804	0.21
Ug-1c	Corapan Rhyolitic Tuff	3541	1911	19014	0.27
Ug-2a	Ignimbrite	3809	2395	22304	0.35

6. Classification of the rock mass

6.1. Definition of geotechnical units

In the rock mass classification, the geological information was taken as a reference. Together with the results of the laboratory tests, the geotechnical units were defined. Based on the above, the classification from Deere and Miller, (1966) was used, which takes into account the simple compressive strength and the Et50 modulus of the intact rock, Figure 6.
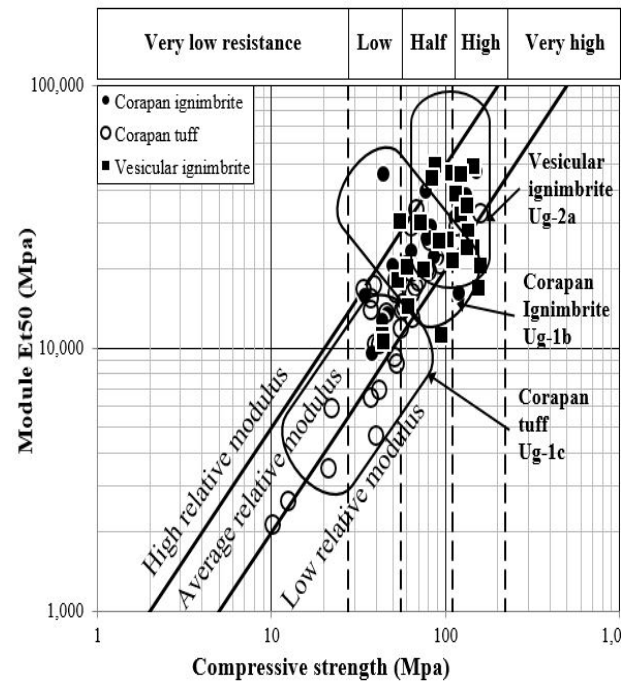

Figure 8. Classification of geotechnical units, Deere-Miller 1966.

6.2. Geological Strength index, GSI

The value of the Geological Strength Index (GSI) was determined using the criteria of Hoek et al. (2013), the parameter JCond89, comes from the joint condition of the Bieniawski's RMR89, classification, from field surveys, using the Eq. (1).

$$GSI = 1.5J_{Cond89} + \left(\frac{RQD}{2}\right) \tag{1}$$

Additionally, the criterion of Morelli (2017) was used to estimate the GSI value Figure 13, which results from plotting the Structure Rating (SR) as a function of the Surface Condition Rating (SCR), where Jv is the joint volumetric index. Rr, Rw and Rf are parameters of the Bieniawski's RMR89 classification, roughness, filling and alteration of the joints respectively, which are described in Eq.s number (2) and (3).

$$SR = 1.75 \ln(J_v) + 79.8 \tag{2}$$
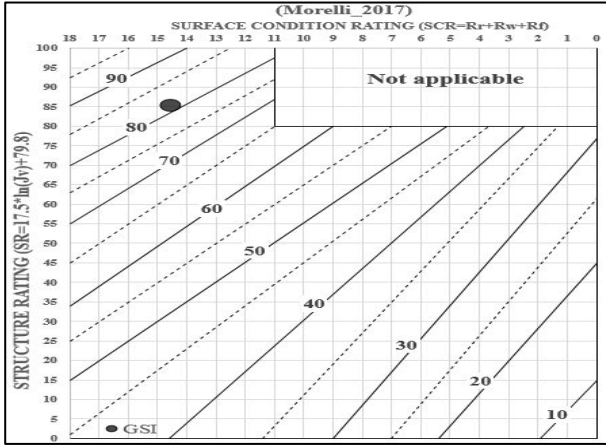
$$SCR = R_r + R_w + R_f \tag{3}$$

3

Figure 9. Calculation of GSI (Morelli, 2017).

7. Evaluation of modules in-situ in the curtain deployment area

In order to evaluate the parameters of rock quality, strength, deformability and alteration in the area of the dam curtain, in situ tests were carried out to analyze the load (E) and dynamic (Ed) modules to evaluate the stability of the structure of the dam curtain, as indicated below.

- Load module.
- Comparison of load modules.

7.1. In-situ testing

In the study zone, seismic refraction lines with (Geophysics) were carried out, obtaining the primary sonic velocity (Vp), deformability tests Goodman jack in drillings (ASTM-D4971, (2025), Aleman J., Chable J. et al, (2017) For the calculation, the load deformability module was considered in Table 1.

To quickly determine the load modulus as a function of the Rock Quality Design (RQD), a graph of the load modulus (E) vs RQD was created (Figure 7).

Table 4. Results of in situ tests the study zone

Lithology	Description	RQD	Sclerometer		E G. jack MPa	Vel., V_p m/s
			R	r		
Ug-1b	Corapan Ignimbrite	80	62	45	6558	4413
Ug-1c	Corapan Rhyolitic Tuff	85	60	42	7522	3541
Ug-2a	Ignimbrite	91	56	42	8950	3809

7.2. In-situ charging module

In order to analyze the behavior of variation in resistance and deformability of the rock mass, the following correlations were made.

- In-situ load modulus vs. Rock Quality Design.
- In-situ load modulus and intact rock vs. Rock Quality Design.

- Dynamic modulos of deformation (Ed) vs Primary velocity (Vp) in-situ.

7.2.1. In-situ load modulus vs. rock quality

In the study area, two boreholes (BR-85 and 91) were carried out, with core recovery to describe the Rock Quality Design (RQD). Subsequently, tests were carried out to record the load modulus in a rock zone using the Goodman jack, which is indicated below.

- Rock Quality Index.
- In-situ loading modulus Goodman jack.

Subsequently, with the results obtained, a correlation of the load module as a function of rock quality (RQD) was carried out, in order to prospect the value of the module at any point in the study area, as indicated in Figure 8, resulting in Eq. number (4).

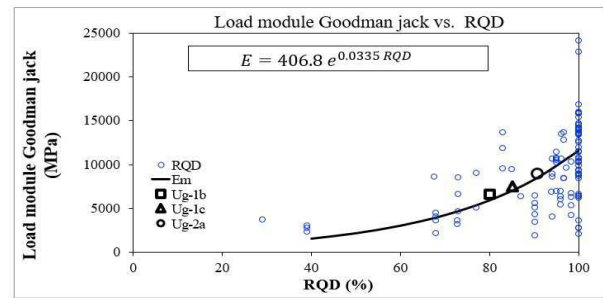$$E = 406.8 \, e^{0.0335 \, RQD} \tag{4}$$

Figure 10. Load module Goodman jack vs RQD

7.2.2. In-situ and intact rock load modules vs. rock quality

For to evaluate the relationship between the in-situ and intact rock loading modules, as a function of rock quality, the following field tests were performed.

- Elasticity Modulus Test (ET_{50}).
- In-situ loading modulus (Rock Pressure Meter, Goodman Jack).

With the results obtained in both tests, a correlation was established between the load module contained in the laboratory and in situ as a function of the rock quality (RQD), in order to explore the degree of alteration of the rock mass with the relationship, as shown in the Figure 9, using equation (5).

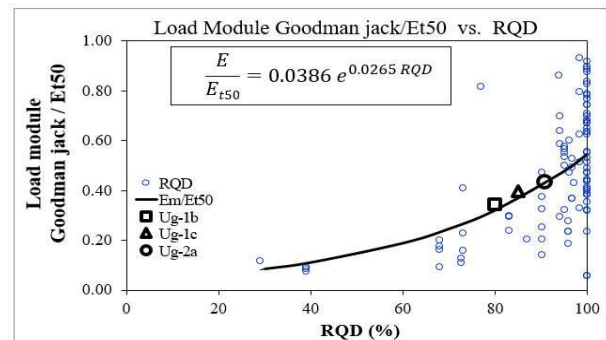$$\frac{E}{Et50} = 0.0386 \, e^{0.0265 \, RQD} \tag{5}$$

Figure 11. Load module Goodman jack / Et50 vs RQD.

7.2.3. Dynamic modulos of deformation (Ed) vs Primary velocity (Vp) in-situ

Because the pressure gauge test is only point-based, the following field tests were performed to evaluate deformability in each of the rock layers in a larger area.

- Seismic Refraction Test.

Based on the previous test, the dynamic modulus (Ed) was calculated from the primary field velocity (Vp) using geophysical tests. The resulting correlation is shown in the Figure 10, which the described in Eq. number (6).
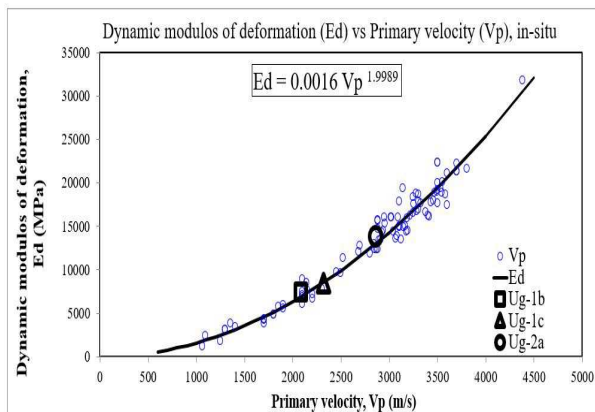
$$Ed = 0.0016\ Vp^{1.9989} \quad (6)$$

Figure 12. Dynamic modulus of deformation vs. primary velocity (Vp).

7.2.4. Comparison of Load Modulus

To analyze the deformability in laboratory and in situ, depending on the degree of weathering and alteration of the rock mass through the Geological Strength Index (GSI), various correlations were used. The most representative is that of Hoek and Diederichs (2006), which takes into account the rock disturbance factor (D), as indicated in the Figure 11 by equation (7).

$$E = E_i \left(0{,}02 + \frac{1 - D/2}{1 + e^{((60 + 15D - GSI)/11)}}\right) \quad (7)$$
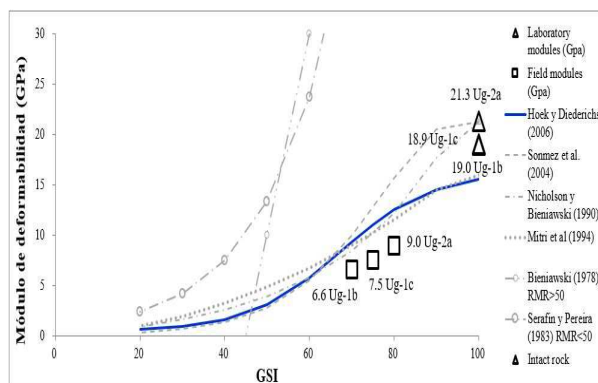

Figure 13. Rock mass deformability (E) vs GSI, (Hoek E., Diederichs, 2006).

8. Hydraulic Properties

To define the hydraulic properties of the rock mass for each rock stratum (1b, 1c, and 2a), a total of 550 Lugeon tests were performed using a 5 m high sealing chamber, applying a constant pressure of 1.0 MPa along the entire length of the boreholes. To analyze the results, a histogram of Lugeon unit values was created according to the Quiñones-Rozo criterion (2010). For better understanding, a whisker box diagram is attached at the top of the graph; the results are shown below.
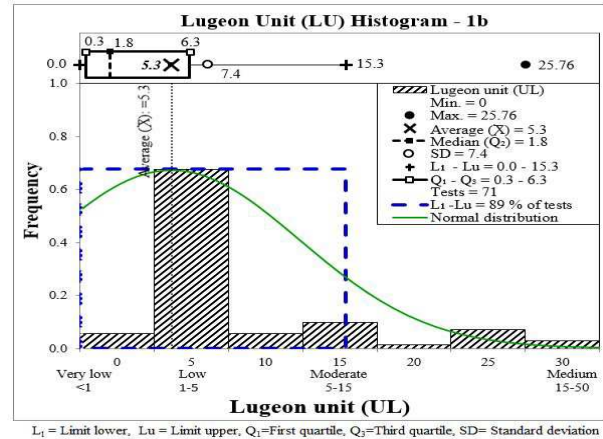

L_1 = Limit lower, Lu = Limit upper, Q_1=First quartile, Q_3=Third quartile, SD= Standard deviation

Figure 14. Histogram of Lugeon unit values from tests performed in stratum 1b.

L_1 = Limit lower, Lu = Limit upper, Q_1=First quartile, Q_3=Third quartile, SD= Standard deviation
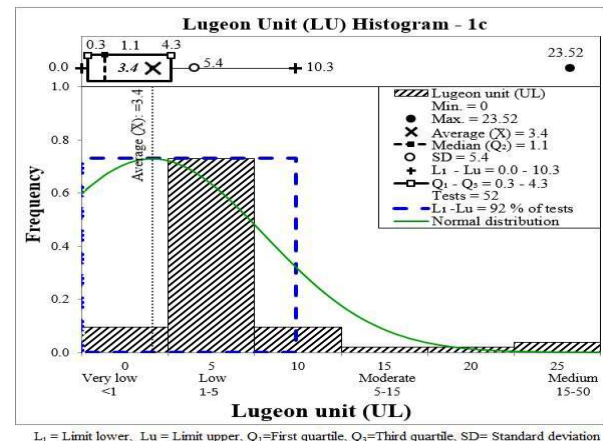
Figure 15. Histogram of Lugeon unit values from tests performed in stratum 1b.

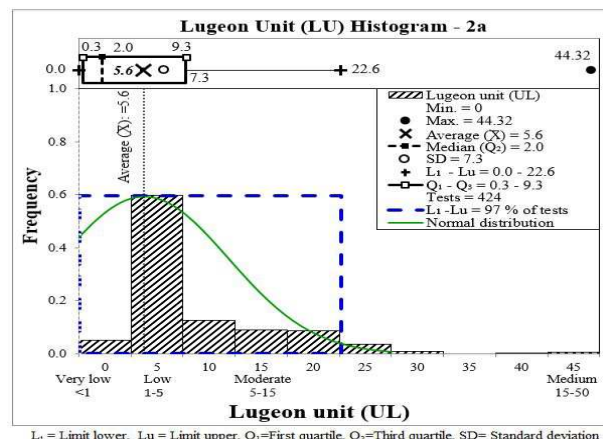L_1 = Limit lower, Lu = Limit upper, Q_1=First quartile, Q_3=Third quartile, SD= Standard deviation

Figure 16. Histogram of Lugeon unit values from tests performed in stratum 2a.

5

Subsequently, in order to examine the variation in Lugeon permeability behavior in relation to Goodman jack deformation, a correlation was made between both results. It is observed that the rock strata (1b, 1b, and 2a) present a range of low to moderate permeability, as indicated in the histograms, considering the interval between the quartiles Q1 and Q3. It is also observed that layer 2a is slightly more permeable because, despite being a very resistant rock, it contains small vesicles, see Table 5 and Figure, resulting in Eq. number (8).

$$E = 23819 \, UL^{-0.434} \tag{8}$$

Table 5. General formatting styles

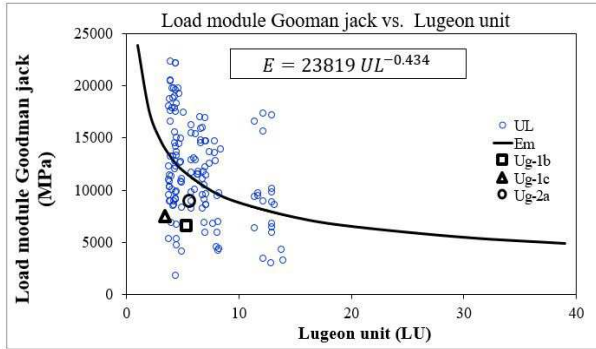| Lithology	E G. jack MPa	Lugeon unit	Coefficient of permeability m/s	Classification
1b	6558	5.3	6.4 E-7	Moderate permeability
1c	7522	3.4	4.0 E-7	Low permeability
2a	8950	5.6	6.8 E-7	Moderate permeability

Figure 17. Load module Goodman jack vs. Lugeon unit.

9. Flow Nets

9.1. Determination of permeability

First, to determine a flow network, it is necessary to have the permeability of the rock layers as data. Therefore, for greater practicality, it is advisable to correlate the permeability tests with the load moduli performed in-situ. This correlation is described in the Figure 13, using Eq. number (9).
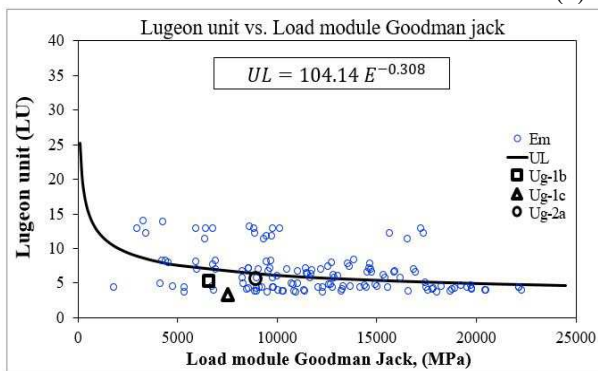
$$UL = 104.14 \, E^{-0.308} \tag{9}$$

Figure 18. Lugeon unit vs. Load module Goodman jack.

9.2. Determination of the Flow Net

The flow network was created using the Laplace continuity theory method (Juarez E., González de Vallejo L, 2002, Das B., 2010), which consists of a graph represented by two sets of orthogonal curves, known as flow lines and equipotential lines. A flow line is the path a water particle follows as it travels from upstream to downstream. An equipotential line is a line along which water registers the same water head. The space between two consecutive flow lines is defined as the flow channel (Nf), and the space between two consecutive equipotential lines is called the drop (Ne), see the Figure 14 and 15.

9.3. Flow net in an isotropic medium

To determine the seepage through the curtain structure, the total water head (H) is considered, which is distributed evenly among the number of equipotential drops (Nd). The total water head (H) is the difference between the upstream head (h_1) contained by the structure and the downstream head (h_2) beyond the structure. The total seepage rate (q) in a flow net in an isotropic medium is given by the following equation,

$$q = K \, H \left(\frac{Nf}{Nd} \right) \tag{10}$$

9.4. Flow net in an anisotropic medium

9.4.1. Seepage Flow Rate in an Anisotropic Flow Net

To determine the flow rate in an anisotropic or stratified medium with different thicknesses (L) and permeabilities (k), an equivalent permeability is defined, representing the flow through the set of layers. This is divided into two components: vertical (Kz) and horizontal (Kx), which are given by Eqs. (11) and (12).

$$K_z = \sum_{i=1}^{n} \left(\frac{L_i}{\frac{L_i}{K_i}} \right) \tag{11}$$

$$K_x = \sum_{i=1}^{n} \left(\frac{K_i L_i}{L_i} \right) \tag{12}$$

The flow rate of the flow net is then calculated using the Eq. number (13).

$$q = \sqrt{K_x K_z} \left(\frac{N_f}{N_d} \right) \tag{13}$$

9.4.2. Methodology for Drawing an Anisotropic Flow Net

The anisotropic flow network is drawn in a transformed medium so that the flow lines and equipotentials meet the Laplace orthogonality conditions, according to the following.

- Draw the geometry of the problem at actual scale, respecting the vertical scale (Sz).
- For the horizontal scale (Sx), use the Eq. number (14).

$$S_z = \sqrt{K_x/K_z}(S_z) \qquad (14)$$

- With the horizontal scale transformed, draw the flow lines and equipotential bonds according to the conditions of an isotropic medium.
- Finally, return the flow network to real space, where the orthogonality conditions will no longer be met.

9.5. Drawing an Anisotropic Flow Net

According to the aforementioned criteria, the flow networks of the diversion works on the right bank and the maximum section of the dam along the riverbed are described, as indicated in the Figures 14 and 15.

9.5.1. Diversion Tunnel Flow Net

This section is aligned in the direction of the diversion tunnel axis, with a length of 400 meters behind the dam structure. It cuts through the rock strata overlying the dam structure's foundation (1b, 1c, and 2a). It has a hydraulic head (H) of 50 meters, generating a maximum filtration rate (q) of 0.10 m³/day/m in stratum 1b, as indicated in Table 6 and Figure 14.

Table 6. Seepage rates of the flow net of the diversion tunnel section

Lithology	E MPa	K m/s	H m	Nf	Nd	q m³/day/m
1b	6558	6.4 E-7	50	3	24	0.10
1c	7522	4.0 E-7	50	1	24	0.10
2a	8950	6.8 E-7	50	6	24	0.06

Em = Goodman Jack, K = Coefficient of permeability, H = Hydraulic Head, Nf = Flow line, Nd = Equipotential line, q = Filtration rate
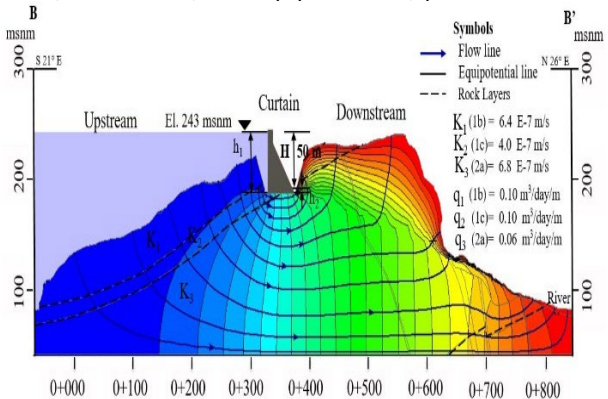

Figure 19. Table 6. Seepage rates of the flow net of the diversion tunnel section.

With the results obtained from the flow net with a hydraulic head of 50 meters, a correlation was made based on tests performed with the pressure gauge, in order to project the filtration rate based on the in-situ rock modulus, which is indicated in Figure 17, using Eq. number (15).

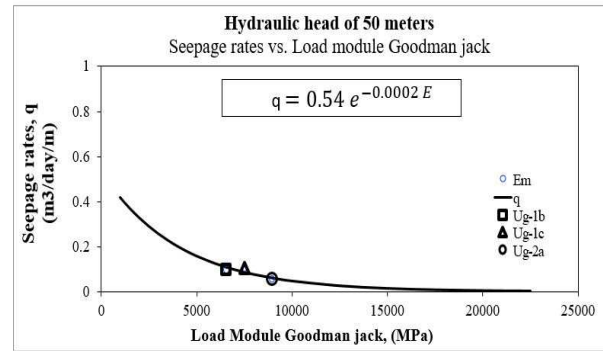$$q = 0.54\, e^{-0.0002\, E} \qquad (15)$$

Figure 20. Table 6. Seepage rates for a hydraulic head of 50 meters.

9.5.2. Flow Net of the Maximum Section

This flow net corresponds to the maximum section of the riverbed of the structure of the Dam, which is aligned to the riverbed, with a length of 500 meters posterior to the structure, it is located on the rock stratum corresponding to unit 2a, which has a thickness of 80 meters to support a maximum water level of 180 meters, which corresponds to a maximum flow of 3.4 m³/day/m, which is illustrated in Table 7 and Figure 15.

Table 7. Seepage rates of the flow network of the maximum section.

Lithology	E MPa	K m/s	H m	Nf	Nd	q m³/day/m
2a	8950	6.8 E-7	180	12	24	**3.42**
2b	13781	6.6 E-7	180	3	24	**0.88**

Em = Goodman Jack, K = Coefficient of permeability, H = Hydraulic Head, Nf = Flow line, Nd = Equipotential line, q = Filtration rate
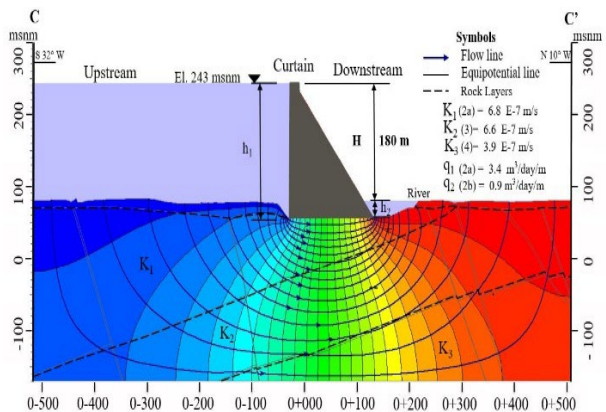

Figure 21. Seepage rates of the flow network of the maximum section of the riverbed.
Figure 22.

Similar to the previous analysis, the filtration rate of the maximum section was projected based on the flow net with a hydraulic head of 180 m, as shown in Figure 19 by equation (16).

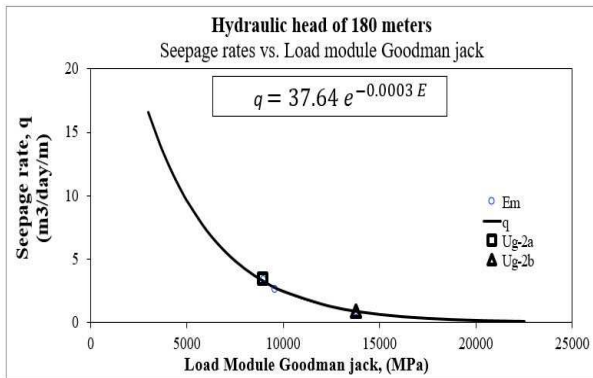$$q = 37.64 \, e^{-0.0003 \, E} \qquad (16)$$

Figure 23. Seepage rates for a hydraulic head of 180 meters.

10. Conclusions

Based on laboratory and in situ tests, along with geomechanical classifications, it was determined that the foundation layer 2a exhibits a rock strength ranging from fair to good, with an RMR between 75 and 80. The most competent zone is found at greater depth, registering an uniaxial compressive strength of the intact rock between 70 and 75 MPa.

To evaluate the rock mass properties, correlations were made between in situ mechanical tests (Goodman Jack) and hydraulic permeability tests. It was determined that modules exceeding 6.5 GPa, with a GSI alteration ranging from 65 to 80, exhibit low permeability, ranging between 3 and 5 Lugeon units, with a permeability coefficient (K) of 4 to 7 x 10^{-4} m/s, defining an environment from slightly permeable to impermeable.

Finally, through flow network analysis, the response of the rock mass was evaluated under a maximum hydraulic head of 180 meters over layer 2a, with a modulus of 8.9 GPa and a permeability of 6.8 x 10^{-4} m/s. Based on these values, a maximum flow rate of 3.5 m³/day/m³ was determined, allowing for the projection of the flow rate based on the field modulus, thus facilitating decision-making regarding the design and treatment of the rock mass during dam construction.

11. References

ASTM D4971. "Standard Test Method for Determining In Situ Modulus of Deformation of Rock Using Diametrically Loaded 76-mm (3-in.) Borehole Jack". ASTM International, 100 Barr Harbor Drive, PO Box C700, West Conshohocken, PA 19428-2959, United States.

Aleman J., Chable J. et al., 2017. "Caracterización geomecánica y tratamientos en los Túneles de Desvío en la margen izquierda del P. H. las cruces, Nayarit". AMITOS, D.F. Mexico. https://issuu.com/amitos/docs/os18_baja/10

Barton N. 2002. "Some new Q-value correlations to assist in site characterisation and tunnel design". International journal of rock mechanics and mining sciences.

Bieniawski, Z. T. 1989. "Engineering rock mass classifications: a complete manual for engineers and geologists in mining, civil, and petroleum engineering". John Wiley & Sons.

Das B. 2002. "Principles of Geotechnical Engineering", Seventh Edition. 200 First Stamford Place, Suite 400, Stamford, CT 06902, USA.

Chable J., Lopez J., 2022. "Adjustment of dispersion values with the Schmidt Hammer". XXXI National Meeting of Geotechnical Engineering, SMIG, Guadalajara, Mexico. https://es.scribd.com/document/734808125/Ajuste-de-valores-de-dispersion-con-el-M

Deere, D. U., & Miller, R. P. 1966. "Engineering classification and index properties for intact rock". Illinois Univ. At Urbana Dept. Of Civil Engineering.

González V. L. 2002. "Ingeniería Geológica", Editorial Pearson Prentice Hall, Pearson Educación., Madrid, España.

Hoek, E., Carranza-Torres, C.T., and Corkum, B. (2002): 2002. "Hoek-Brown failure criterion", edition. Proc. North American Rock Mechanics Society.

Juarez V. E., Rico R. A. 1974. "Mecánica de suelos tomo III, Flujo de agua en suelos", Editorial Limusa, D.F., Mexico.

Miller, R.P. 1965. "Engineering classification and index properties for intact rock". Ph.D. Thesis univ. Ill, 1- 322 P.

Montiel E., Chable J. 2012. "Geomechanical characterization of ignimbrite sequence. Site of the Hydroelectrical project, Las Cruces", XXVI National Meeting of Geotechnical Engineering, SMIG, Cancun, Mexico. https://aprenderly.com/doc/987637/paper-title---sociedad-mexicana-de-ingenier%C3%ADa-geot%C3%A9cnica

Morelli, G. L. 2017. "Alternative Quantification of the Geological Strength Index Chart for Jointed Rocks", Springer International Publishing AG.

Quiñones-Rozo C. 2010. "Lugeon test interpretation, revisited", URS Corporation, 1333 Broadway Suite 800, Oakland, CA 94612.

INTERNATIONAL SOCIETY FOR SOIL MECHANICS AND GEOTECHNICAL ENGINEERING

The paper was published in the proceedings of the 8th International Symposium on Pressuremeters (ISP2025) and was edited by Wissem Frikha and Alexandre Lopes dos Santos. The conference was held from September 2nd to September 5th 2025 in Esch-sur-Alzette, Luxembourg.